Available online at www.sciencedirect.com
SCIENCE DIRECT®
PERGAMON
International Journal of Heat and Mass Transfer 46 (2003) 2015–2026
International Journal of HEAT and MASS TRANSFER
www.elsevier.com/locate/ijhmt

Cooling of cylindrical vertical tanks submitted to natural internal convection

Rejane De Césaro Oliveski [a,*], Arno Krenzinger [b], Horácio A. Vielmo [c]

[a] Centro de Ciências Exatas e Tecnológicas, Universidade do Vale do Rio dos Sinos, Engenharia Mecânica Av. Unisinos, 950. CEP: 930220-000 São Leopoldo, RS, Brazil

[b] Departamento de Engenharia de Materiais, Universidade Federal do Rio Grande do Sul Rua Sarmento Leite, 425. CEP: 90050-170 Porto Alegre, RS, Brazil

[c] Departamento de Engenharia Mecânica, Universidade Federal do Rio Grande do Sul Rua Sarmento Leite, 425. CEP: 90050-170 Porto Alegre, RS, Brazil

Received 28 November 2001; received in revised form 16 October 2002

Abstract

A numerical and an experimental analysis of velocity and temperature fields inside a storage tank submitted to natural convection is presented. The analysis was performed in two stages. In the first stage, the temperature profile along the vertical axis of the storage tank was obtained experimentally and numerically, for cooling time ranging from 45 to 60 h. The numerical analysis was carried out using a transient bi-dimensional model in cylindrical co-ordinates. In the second stage, after the numerical code validation, 40 cases of cooling with four aspect ratios, five insulation thicknesses, and two different volumes were simulated. In all simulations, thermal losses for the environment in all tank walls (side, top and bottom) were considered. Two correlations for the Nusselt number, encompassing all the forty cases, were obtained with these results.

1. Introduction

Many sectors of engineering, such as the petrochemical industry, food industry and liquid heating systems, use thermal storage to optimize the performance of their systems. This effective optimization requires an extensive knowledge of the thermal behavior of tanks, and the relationship of the fluid with the tank walls and thermal insulation. Both in the heating and cooling processes, heat is transferred within the tank by diffusive effects in certain regions and advective effects in others. The most simplified models that attempt which try to reproduce the thermal behavior of a tank use only heat diffusion among the different fluid layers. However, they fail when it is necessary to describe in detail the temperature profile of the stored fluid. The differences observed between experimental analysis and results of the simplified models show the need of implementing detailed numerical models to determine the actual temperature distribution. Recent studies show the progress of this subject in the specialized literature.

Researchers divide their attention between numerical models that deal with mass conservation, momentum and coupled energy equations [1–4], and less generic models, which usually use only a single energy balance equation to determine the temperature profile within the storage tank [5,6].

Reindl et al. [1] analyzed transient natural convection in vertical cylindrical tank with perfect insulation at the top. Initially, the fluid in the is isothermal and quiescent. At time zero, a step change in the source temperature begins to influence the flow. The average Nusselt number was presented during a maximum time of 1000 s for several Rayleigh numbers. Considering cooling of an oil tank, Cotter and Charles [2] used the mean temperature of the liquid, the wall temperature, and the cold ambient temperature to obtain the average Nusselt number. In

* Corresponding author. Tel./fax: +55-51-33312118.
E-mail address: decesaro@ufrgs.br (R. De C. Oliveski).

0017-9310/03/$ - see front matter © 2003 Published by Elsevier Science Ltd.
doi:10.1016/S0017-9310(02)00508-2

Nomenclature

A	area (m^2)
c_p	specific heat at constant pressure ($J\,kg^{-1}\,K^{-1}$)
D	diameter (m)
e	insulation thickness (m)
F_s	safety coefficient of the *grid convergence index* (–)
g	gravitational constant ($m\,s^{-2}$)
h	external heat transfer coefficient ($W\,m^{-2}\,K^{-1}$)
h_z	local internal heat transfer coefficient ($W\,m^{-2}\,K^{-1}$)
$\bar{h}$	average heat transfer coefficient of the tank ($W\,m^{-2}\,K^{-1}$)
H	total height (m)
k	thermal conductivity ($W\,m^{-1}\,K^{-1}$)
L	characteristic length (m)
m	number of volumes in the radial direction (–)
n	number of volumes in the axial direction (–)
Nu	local Nusselt number (–)
p	pressure (Pa)
$\bar{q}''$	average heat flux ($W\,m^{-2}$)
Q_{Tot}	total heat flux ($W\,m^{-2}$)
r	radius (m)
R	total radius (m)
t	time (s)
T	temperature (°C)
$\overline{T}_z$	average temperature of the cross section of the tank (°C)
$T_{z,R}$	wall temperature (°C)
$\overline{T}_{3/4,r}$	average temperature of the ring between 3/4 of H and H (°C)
$\overline{T}_{H/4,r}$	average temperature of the ring (°C)
$\overline{T}$	average temperature of the fluid (°C)
$\overline{T}_w$	average temperature of the internal face of the tank walls (°C)
u	axial velocity ($m\,s^{-1}$)
U^*	global heat transfer coefficient ($W\,m^{-2}\,K^{-1}$)
v	radial velocity ($m\,s^{-1}$)
z	axial position (m)

Greek symbols

α_r	grid refinement coefficient in radial direction (–)
α_z	grid refinement coefficient in axial direction (–)
ΔT	temperature difference (K)
μ	dynamic viscosity ($kg\,m^{-1}\,s^{-1}$)
ρ	density ($kg\,m^{-3}$)

Subscripts

amb	ambient
B	bottom
S	sidewall
T	top
w	wall

that study, the authors presented the time dependence of Nusselt for several oil viscosity values. Lin and Armfield [3] numerically simulated cooling in a vertical cylindrical tank with perfect insulation at the top and bottom. The initial condition used in the simulation was isothermal field; the transient regime was obtained with a sudden temperature decrease on the sidewall. In that study, the authors presented results of the required time to reach a determined stratification condition as a function of the Rayleigh number (2×10^7–1×10^9). Natural convection was also analyzed by Ivancic et al. [4], who used perfect insulation outline conditions on the side of the tank, while maintaining low temperature at the top, and high temperature at the bottom, thus forcing a Rayleigh–Bérnard type convective pattern. Gross [7], Zurigat et al. [8], Murthy et al. [9] and Nelson et al. [10] investigated the degradation of thermal stratification in vertical cylindrical tanks under mixed convection conditions, starting with an initial condition of uniform temperature field in thermocline. Murthy et al. [9] studied the influence of thermal conduction through storage tank walls in three tanks built with different materials and two different wall thicknesses. These authors were able to express the coefficient of mixture by the Reynolds and Richardson numbers, instead of the traditional empirical coefficients of mixture presented by Oppel et al. [11], Cole ad Bellinger [12] and Al-Najem et al. [13].

The present study aims at investigating, numerically and experimentally, natural convection by cooling of vertical cylindrical storage tanks submitted to heat transfer to the environment in all tank walls (top, bottom and side). After the validation of the numerical model with experimental results, the cooling of the tanks is simulated under forty different configurations, obtaining correlations of the Nusselt number as a function of the thermal losses to the environment, aspect ratio and tank volume.

2. Experimental apparatus

The experimental tests were performed in a vertical cylindrical tank made of stainless steel, measuring 57 cm height, 21 cm of radius, and 1 mm wall thickness, was used. The materials of the metallic structure and thermal insulation of the tank are identified in Fig. 1(a).

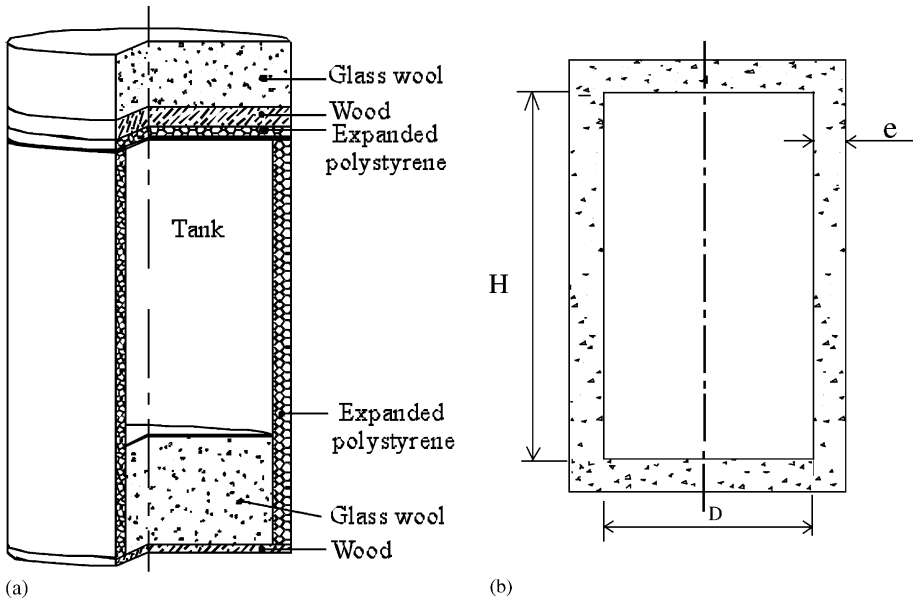

Fig. 1. The storage tank: (a) experimentally analyzed and (b) generic.

In order to measure the internal tank temperature, iron-constantan type thermocouples of 0.125 mm diameter were used. The uncertainty analysis, considering the measurements of temperature, effects of time and positions of thermocouples and data connection board, resulted in a mean uncertainty of ±0.27 °C, evaluated as according to Moffat [14].

In order to assist temperature sensors handling, the insulation of the top of the tank consisted of a 10 mm expanded polystyrene. Thermal insulation of the top is complemented by 12 mm glass wool, as seen in Fig. 1(a). Water surface was covered with plastic sheet and expanded polystyrene lid lined with impermeable material to minimize evaporation losses.

Tests were carried out at the Solar Energy Laboratory of the Federal University of Rio Grande do Sul, which is submitted to environmental temperature variations. This temperature was monitored by two PT100 transducers. Environmental temperature was used as reference for thermocouples and as boundary condition for numerical simulation. All tests started with uniform water temperature within the tank. Temperatures were 51.5 °C, 72.5 °C and 82 °C, and times of monitoring were 15 h, 60 h and 45 h, respectively.

3. Numerical approach

Natural convection regime experiments were simulated with equations of continuity, momentum in axial and radial directions, and energy. These equations are shown below (1)–(4)

$$\frac{\partial \rho}{\partial t}+\frac{\partial(\rho u)}{\partial z}+\frac{1}{r}\frac{\partial(\rho r v)}{\partial r}=0 \tag{1}$$

$$\frac{\partial(\rho u)}{\partial t}+\frac{\partial(\rho u u)}{\partial z}+\frac{\partial(\rho v u)}{\partial r}=-\frac{\partial p}{\partial z}+\mu\left(\frac{\partial^2 u}{\partial z^2}+\frac{1}{r}\frac{\partial u}{\partial r}+\frac{\partial^2 u}{\partial r^2}\right)+\rho g \tag{2}$$

$$\frac{\partial(\rho v)}{\partial t}+\frac{\partial(\rho u v)}{\partial z}+\frac{\partial(\rho v v)}{\partial r}=-\frac{\partial p}{\partial r}+\mu\left(\frac{\partial^2 v}{\partial z^2}+\frac{1}{r}\frac{\partial v}{\partial r}+\frac{\partial^2 v}{\partial r^2}-\frac{v}{r^2}\right) \tag{3}$$

$$c_p\left[\frac{\partial(\rho T)}{\partial t}+\frac{\partial(\rho u T)}{\partial z}+\frac{\partial(\rho v T)}{\partial r}\right]=k\left[\frac{\partial^2 T}{\partial z^2}+\frac{1}{r}\frac{\partial T}{\partial r}+\frac{\partial^2 T}{\partial r^2}\right] \tag{4}$$

where ρ is the density, u and v are the axial and radial velocity, T is the temperature, μ is the dynamic viscosity, k is the thermal conductivity, c_p is the specific heat at constant pressure, p is the pressure. In the above equations, ρ is considered as an unknown in all terms.

3.1. Boundary and initial conditions

For the momentum equations, impermeability and no slip conditions in every wall, including the symmetry line, since the thermocouples were located in those positions, were adopted.

In the energy equation, the computational domain was extended up to the thermal insulation, including the

metallic wall. The boundary condition of the third kind was used, i.e., every tank wall (side, bottom and top) was submitted to external convection action, and the mean convection heat transfer coefficient used was 10 W/m^2 K. This coefficient describes the situation assayed in the laboratory and it represents common practical situations (Cotter and Charles [2], $h = 11$ W/m^2 K; Adhikari et al. [15], $h = 9.5$ W/m^2 K). Although variations of these values may be possible, their effect would be much attenuated, as the composition of the global heat transfer coefficient takes into consideration two serial thermal resistances, where the highest value corresponds to the insulation resistance. In order to complete the boundary condition of the third kind, experimental records of environmental temperature, transformed into time-dependent polynomials, were used.

3.2. Methodology

The numerical solution was obtained by integrating the Eqs. (1)–(4) in Finite Volumes, as described by Patankar [16], Veersteg and Malalasekera [17], Ferziger and Periç [18]. Pressure–velocity coupling was obtained by the SIMPLEC, Van Doormaal and Raithby [19]. The Power Law scheme of Patankar [20] was used for the interpolation in the control volume faces. Although there are other available schemes, the Power Law was used in all simulations because it has been proven robust, with good numerical stability. Under this scheme, grid independence was verified by the grid convergence index (GCI), according to Roache [21]. The resulting equation systems were solved by TDMA. The convergence criterion requires that the normalized mass flow residue for any grid volume to be lower or equal to 10^{-4} kg/s. Aiming at accelerating convergence, diffusing more efficiently the influence of the boundary conditions to the inside of the domain, a block correction was used to calculate velocity and temperature components.

The equation generating the used grid was suggested by Davidson [22], which, for axis symmetry direction, was refined in both extremities. This equation is presented below:

$$z_i = L\left\{ -0.5\tan h\left[\alpha_z\left(2\frac{i-2}{n-2}-1\right)\right]\Big/\tan h(-\alpha_z) + 0.5\right\} \quad (5)$$

where $2 \leqslant i \leqslant n$, where n is the number of volumes in the axial direction, and α_z is the grid refinement coefficient in the axial direction.

In the radial direction, grid refinement is made only at the sidewall, and is obtained by:

$$r_j = R\left\{\tan h\left[\alpha_r\left(\frac{j-2}{m-2}\right)\right]\Big/\tan h(-\alpha_r)\right\} \quad (6)$$

where $2 \leqslant j \leqslant m$, where m is the number of volumes in the radial direction, and α_r is the grid refinement coefficient in radial direction. These equations discretize only the water volume. The computational domain included the water contained in the tank, the metal structure, including its wall, and the thermal insulation of the tank. The thermal problem was solved taking into consideration the thermophysical properties of all of these items, the diffusion heat transfer through the metal walls and thermal insulation, both in the radial and axial directions. The influence of the heat transfer by diffusion on the metal wall along the height of the tank tends in fact to smear the thermocline. However, this is not significant for the usual wall thickness, as investigated by Bandini and Vielmo [23].

All equations refer to the same computational domain. Volumes corresponding to the metallic structure and thermal insulation are immobilized.

Only the thermal conductivity was used as the coefficient of diffusion in the energy equation, and c_p was maintained in the advection and time terms, along with the density. This procedure was adopted because the solution uses the harmonic average to obtain effective thermal conductivity in the volume interface, and c_p does not participate directly in the heat transfer by diffusion between two neighboring control volumes.

4. Validation of the bi-dimensional model

Several tests with an initial condition of uniform temperature were carried out. The first cooling results were obtained with an initial temperature field of 50 °C. The other tests were conducted with higher initial temperatures, with increases of ≈10 °C.

The comparison between experimental and numerical data is shown in Fig. 2, where the formation of stratification during the cooling of the tank is observed by the temperature profile at the center. The figure shows that, even 60 h after cooling, the numerical simulation is able to reproduce the experimental data with excellent accuracy. At the bottom region, we can also observe a marked increase of the thermal gradient in the vertical direction. The same behavior was observed in the study of Abdoly and Rapp [24], where the authors suggest that this sudden drop in temperature is due to conductive losses through the metallic columns of the tank. However, they do not make any quantitative remarks.

5. Applications

After experimental validation and evaluation of grid independence, the developed numerical model was then used to simulate the cooling of the tank under different aspect ratios and thermal losses to the environment. This stage aimed at obtaining the Nusselt number for

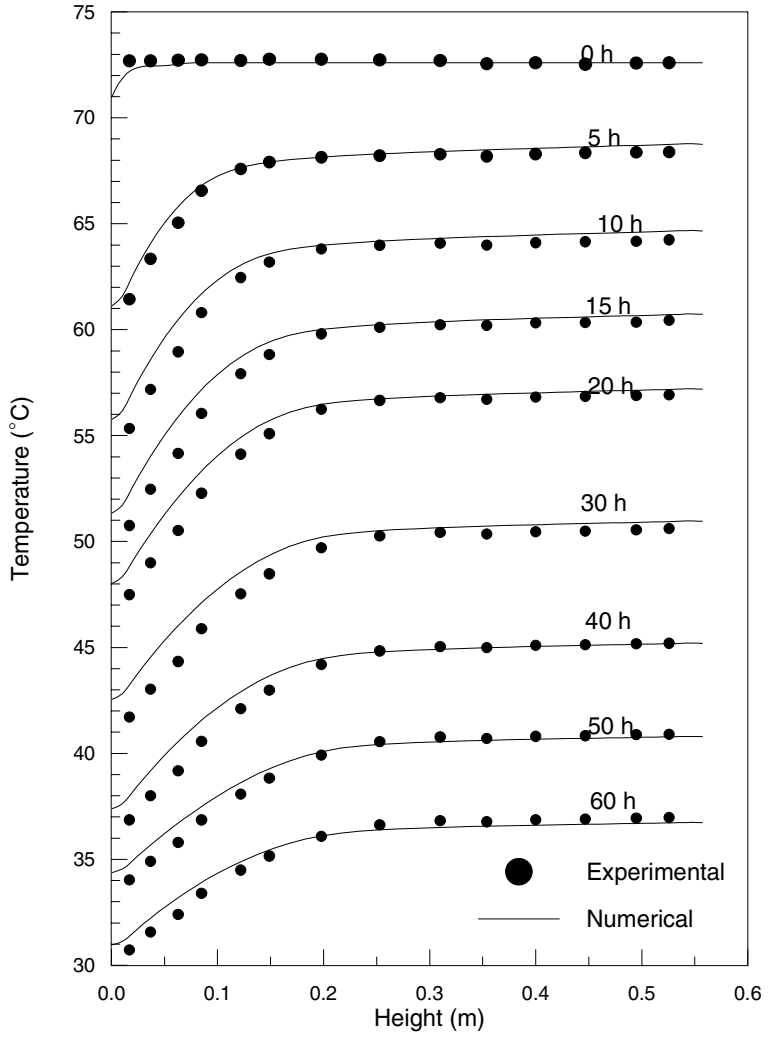

Fig. 2. Temperature profiles at the center of the tank with initial uniform temperature of 72.5 °C.

the free convection inside this type of tank, correlated by the tank aspect ratio and thermal losses to the environment.

The storage tank studied at this stage had the same geometry of the previously studied tank, i.e., it was vertical and cylindrical. However, aiming at the generalization of the problem, the structural peculiarities of that tank (inferior wing and superior collar) were abandoned. In this analysis, the tank consisted of only two materials. The metallic structure was made of stainless steel and the thermal insulation was made of glass wool. Its generalized structure can be seen in Fig. 1(b), where "e" is the insulation thickness; H is the height, and D the diameter of the tank.

The boundary conditions are the same as those used to simulate the previously mentioned cases, except for the axial velocity at the center of the tank. For that cooling case, a non-slipping condition was used, whereas in the cases considered here, the symmetry condition was used, i.e., null derivative relative to the radius for axial velocity at the centerline. An isothermal field equal to 70 °C was used as initial condition for temperature.

In this analysis, forty different configurations were used with respect to tank volume, aspect ratio (H/D) and insulation thickness (e). For tanks volumes of 0.1 and 0.3 m^3, four aspect ratios were used: 1.0, 1.5, 2.0, and 2.5. Each of these aspect ratios had five different insulation thicknesses: 4, 3, 2, 1 and 0.1 cm, with a total of forty cases.

5.1. Grid independence study

The magnitude of the heat flux at the tank walls determine the degree of grid refinement needed to obtain

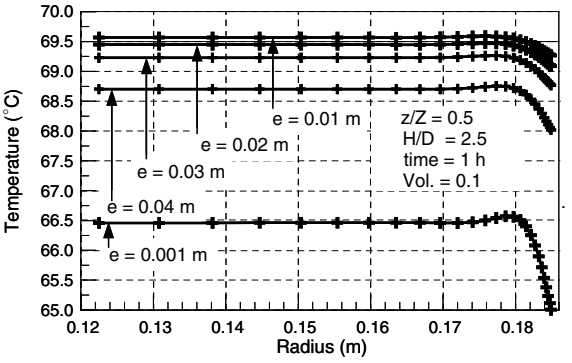

Fig. 3. Temperature profiles along the radius.

a stable solution; that is the larger the thermal gradients found in these regions, the higher the number of volumes is needed. To quantify this assertion, temperature profiles along the tank radius at $0.5H$ are presented in Fig. 3, where all profiles were calculated for a 0.1 m^3 tank with an aspect ratio (H/D) of 2.5, and five different thicknesses.

Fig. 3 shows that the temperature is quasi-constant along the radius. As expected, there is a thermal boundary layer in the wall, where heat is removed. The difference among thermal gradients for different thicknesses is observed near the wall. The curve corresponding to the insulation thickness $e = 4$ cm shows a difference in temperature between the wall and the center of the tank of $\approx$0.75 °C, whereas for an insulation of 0.1 cm, the difference is 1.5 °C, with no proportional enlargement of the boundary layer, resulting in much larger temperature gradient.

As already seen in Kimura and Bejan [25] and Bandini and Vielmo [23], a temperature increase is seen before the thermal boundary layer itself is observed, particularly when there is larger heat loss. This results from the fact that the descending liquid comes from higher regions in the tank, where the temperature is also higher. Since this liquid is not as close to the wall as that of the thermal boundary layer, it is not cooled at the same rate, and maintains relatively higher temperatures.

The symbols superimposed on the curves are located in the center of each adopted grid volume. In Fig. 3, it is observed that the curve representing the most intense cooling ($e = 0.1$ cm) has 16 volume elements before a constant value is reached. Although this number of elements is sufficient to capture the thermal boundary layer, cases considering to more intense cooling were submitted to grid dependence analysis. The other cases were not analyzed, as they have less intense cooling regimes.

In more intense cooling rates ($U^* = 8$ W/m^2 K), 16 volumes elements were placed inside the thermal boundary layer, with a grid of 40×60 elements in the radial and axial directions, respectively. Although this number of elements is sufficient to identify the existing gradients in the thermal boundary layers, as can be seen in Fig. 3, these cases were submitted to grid dependence analysis, comparing 40×60 to 60×90 volume grids. The other cases were not submitted to this analysis, as the cooling rates were less intense, requiring less spatial and temporal discretization. In addition, time steps of 0.5, 1 and 2 s were tested. Insignificant differences were observed among the results obtained with time intervals of 1 and 2 s. The results obtained with time intervals of 0.5 and 1 s was coincident, according to the limit of figure resolution. CPU time was very high for the time interval of 0.5 s. Therefore it was decided to simulate all cases, including those with less intense cooling, with the time interval of 1 s.

The GCI, Roache [21], with a safety factor equal to three was applied for grid dependence analysis. Grid dependence was investigated with respect to the average temperature of the tank as a function of time and also at the point of maximum variation among the solution obtained for different grids. The results of temperature profile along the tank height and time showed that the maximum distance among solutions occur at the thermocline.

The calculated GCI in the region of thermocline for temperatures at the center of the tank presented maximum value of 3%. Two factors must be taken into account in this observation. First, the GCI had a maximum safety coefficient of $F_s = 3$, i.e., the error was overestimated. Secondly, the analyzed cooling was very intense, with a global heat transfer coefficient (U^*) of 8 W/m^2 K, defined as follows:

$$U^* = \frac{1}{\frac{e}{k} + \frac{1}{h}} \tag{7}$$

This coefficient takes into account only the resistances derived from thermal insulation and external convection of the tank (h). Although this concept is employed in approaches where the domain is not discretized, the main objective here was to determine the heat transfer coefficient by convection between the fluid and the internal face of the tank, which was unknown until then. Once this was determined, correlations of Nusselt could be obtained for the entire tank, a parameter that is of great interest and one of the objectives of this study.

The variation in the average temperature of the tank as a function of different grids was also analyzed by GCI. In this case, the results were 0.3%, which is much more satisfactory.

5.2. Local heat transfer coefficient

The heat transfer coefficient is presented here in two ways. In the first, it is defined in order to present local

results for the side, top and bottom of the tank. In the second, its average value is presented by correlations that take into account the tank aspect ratio, the difference between average and the environmental temperatures, and the thermal losses to the environment.

5.2.1. Heat transfer coefficient at the sidewall

The reference temperature difference ΔT that was used to obtain the heat transfer coefficient (Eq. (8)) is the difference between the average temperature of the cross section of the tank ($\overline{T}_z$) and the sidewall temperature ($T_{z,R}$), at the same height, as shown in Eq. (8).

$$\Delta T = \overline{T}_z - T_{z,R}, \quad \overline{T}_z = \frac{1}{\pi R^2}\int_0^R T|_{z=z} 2\pi r \,\mathrm{d}r \tag{8}$$

$$h_z = \frac{k}{\Delta T}\left.\frac{\partial T}{\partial r}\right|_{r=R}, \quad Nu_z = \frac{h_z z}{k} \tag{9}$$

The Nusselt number calculated by Eq. (9) is shown in Fig. 4(a). The results for aspect ratio of $H/D = 2$, volume of 0.2 m^3, and three values of global heat transfer coefficient (U^*): 1.0, 1.8 and 2.9 W/m^2 K are presented for 1 h and 30 min of cooling. As seen, both qualitative and quantitative characteristics were very similar, regardless the case and the cooling time. The main differences were found at the bottom of the tank. This can be explained with the aid of Fig. 5, which presents the same cases of Fig. 4(a), but illustrates the local internal heat transfer coefficient instead of the Nusselt number along the tank height. In terms of curvature, three different regions can be observed in Fig. 5: bottom, middle and top. The curve characteristics remained almost unchanged at the middle and at the top, despite differences between these regions. As for the bottom, the space limit of this region advanced with time, and this space was given by the side of the tank.

According to Oliveski [26], the thermocline progressed to the top, a region that was dominated by conduction and whose that temperature was homogeneous in all radius extension. Therefore, it can be concluded that the high value of the heat transfer coefficient near the bottom relative to half the height of the tank was due to the very small reference ΔT, and not because the temperature gradient near the wall was very high. The increase of the heat transfer coefficient near the top, relative to half the height of the tank, is explained by the high thermal gradient in that region.

5.2.2. Heat transfer coefficient at the top

During cooling, the thermal behavior of the tank was characterized by the progress of the thermocline to the top, as can be seen since Fig. 2. Therefore, it is suggested that the average temperature that was most representative of the top region was located between $3/4H$ and H. Hence, the reference ΔT for the top of the tank is obtained by:

$$\Delta T = \overline{T}_{3/4,r} - T_{H,r}, \quad \overline{T}_{3/4,r} = \frac{1}{H/4}\int_{3H/4}^{H} T|_{r=r}\,\mathrm{d}z \tag{10}$$

where $\overline{T}_{3/4,r}$ is the average temperature of the ring between $3/4H$ and H, and $T_{H,r}$ is the local temperature at the top. The heat transfer coefficient (h_T) and the local Nusselt number at the top (Nu_T) are obtained as follow:

$$h_T = \frac{k}{\Delta T}\left.\frac{\partial T}{\partial z}\right|_{z=H}, \quad Nu_T = \frac{h_T r}{k} \tag{11}$$

Fig. 4(b) shows the local Nusselt number at the top of the tank in cases with volume of 0.2 m^3, and global heat transfer coefficients (U^*) of 1, 1.3 and 8 W/m^2 K. For each of these cases, Nu_T results are plotted after 1, 8 and 30 h of cooling. As in the case of the local Nusselt number at the side (Nu_S), the solutions are similar to each other, independent of the analyzed case and the cooling time.

The thermal and hydrodynamic behavior at the top of the tank is similar to the Rayleigh–Bénard cells in heat transfer between horizontal level plates, where the inferior plate has high temperature, and the superior plate has low temperature. The water at the top of the tank losses heat to the environment, it increases its density and descends to the lower level where it finds the same density. Due to mass conservation, other portions of water must go up. Therefore, circulations are found at the top of the tank. This probably is the reason for the oscillations between the solutions observed in the Fig. 4(b). This behavior also justifies the wider amplitudes of the case of highest global heat transfer coefficient.

5.2.3. Heat transfer coefficient at the bottom

The reason why the tank is divided into parts, as mentioned in the previous item, is also used here to determine the reference ΔT. In this case, it is obtained by the difference between the average temperature of the ring ($\overline{T}_{H/4,r}$) and local temperature at the bottom of the tank ($T_{0,r}$):

$$\Delta T = \overline{T}_{H/4,r} - T_{0,r}, \quad \overline{T}_{H/4,r} = \frac{1}{H/4}\int_0^{H/4} T|_{r=r}\,\mathrm{d}z \tag{12}$$

The local heat transfer coefficient at the bottom (h_B) and the corresponding Nusselt number (Nu_B) were obtained by:

$$h_B = \frac{k}{\Delta T}\left.\frac{\partial T}{\partial z}\right|_{z=0}, \quad Nu_B = \frac{h_B r}{k} \tag{13}$$

The Nusselt number obtained by this equation is shown in Fig. 4(c) for an aspect ratio of 2.5 and a volume of 0.1 m^3 for different global heat transfer coefficients and cooling times. The figure shows that the Nusselt number as defined in Eq. (13) were qualitatively similar, regardless the analyzed case, but that they were time-dependent.

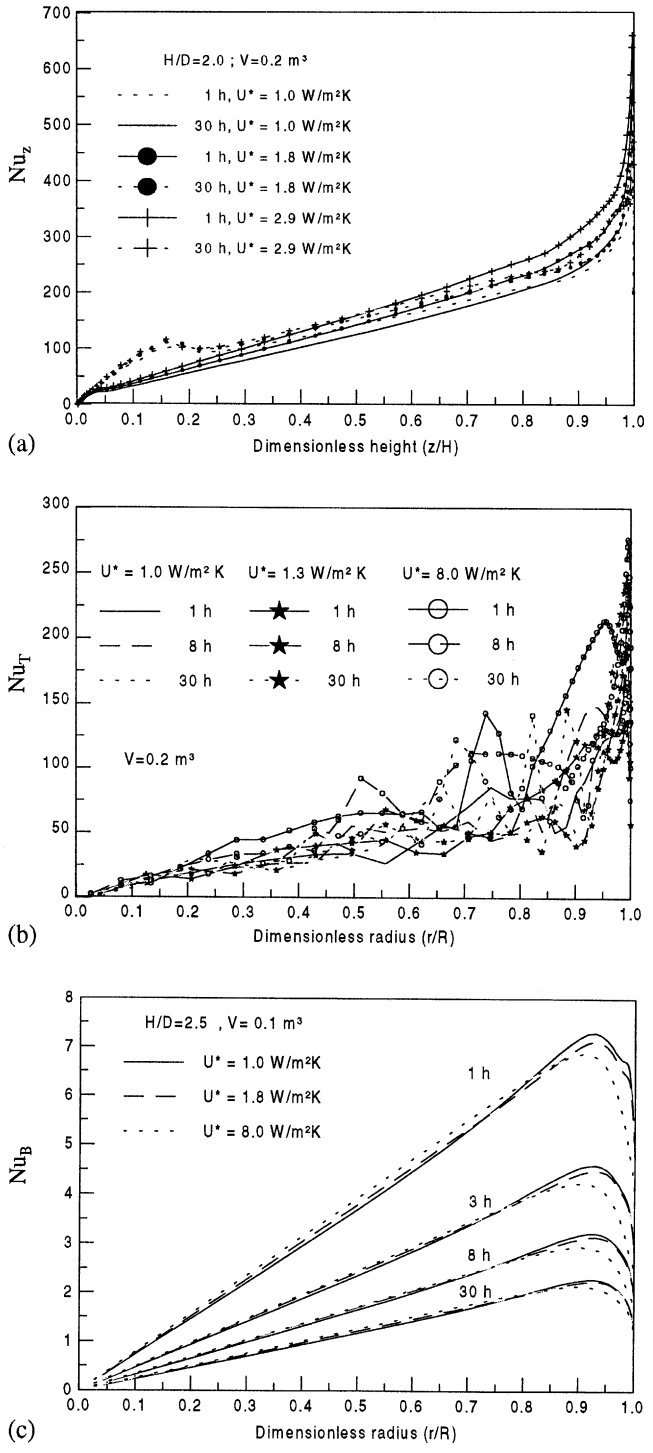

Fig. 4. Local Nusselt number: (a) sidewall, (b) top and (c) bottom.

In Fig. 4(c), it is seen that, for r/R less than 0.8, the Nusselt number for the case of $U^* = 8.0$ W/m^2 K was slightly higher than $U^* = 1.8$ W/m^{2}K, and that, for the positions closer to the sidewall, this behavior is inverted. The first case results from the thermal gradient in the axial direction being higher for of $U^* = 8.0$ W/m^2 K in

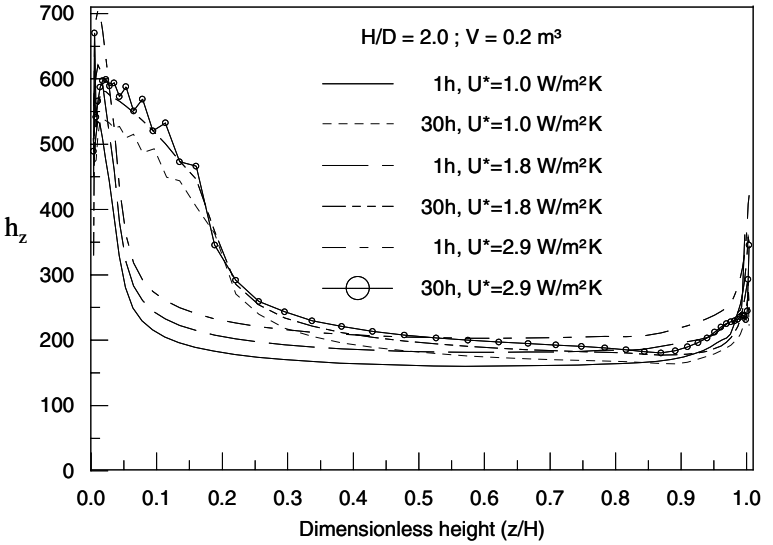

Fig. 5. Local heat transfer coefficient of sidewall.

comparison to $U^* = 1.8$ W/m^2 K, therefore increasing the Nusselt number. As for the region close to the sidewall, the same behavior would be seen if it were insulated. Since it was not, there was a larger transference of heat to the external environment, and this transference had the same intensity in both directions, axial and radial. Hence, the thermal gradient of the axial direction, obtained by the calculation of the Nusselt number, decreased.

5.3. The average heat transfer coefficient

The average heat transfer coefficient of the tank ($\bar{h}$) takes into account the total heat flux (Q_{Tot}), i.e., the sum of heats exchanged by the side, bottom and top. The considered temperature difference is between the average fluid temperature ($\overline{T}$) and the average temperature of the internal face of the tank walls ($\overline{T}_{\mathrm{w}}$), presented in Eqs. (14) and (15), respectively.

$$Q_{\mathrm{Tot}} = A_{\mathrm{S}}\bar{q}''_{\mathrm{S}} + A_{\mathrm{B}}\bar{q}''_{\mathrm{B}} + A_{\mathrm{B}}\bar{q}''_{\mathrm{B}}, \quad \bar{h} = \frac{Q_{\mathrm{Tot}}}{A_{\mathrm{Tot}}(\overline{T} - \overline{T}_{\mathrm{w}})} \tag{14}$$

$$\overline{T} = \frac{1}{\pi R^2 H}\int_0^H \int_0^R 2\pi r T \,\mathrm{d}r\,\mathrm{d}z,$$
$$\overline{T}_{\mathrm{w}} = \frac{A_{\mathrm{S}}\overline{T}_{\mathrm{S}} + A_{\mathrm{B}}\overline{T}_{\mathrm{B}} + A_{\mathrm{T}}\overline{T}_{\mathrm{T}}}{A_{\mathrm{S}} + A_{\mathrm{B}} + A_{\mathrm{T}}} \tag{15}$$

where A_{S}, A_{B} and A_{T} are the areas of the side, bottom and top walls, respectively. The average heat flux and the average temperature of the side, top and bottom walls are obtained by the Eqs. (16)–(18), respectively.

$$\bar{q}''_{\mathrm{S}} = \frac{1}{H}k\int_0^H \left.\frac{\partial T}{\partial r}\right|_{r=R} \mathrm{d}z, \quad \overline{T}_{\mathrm{S}} = \frac{1}{H}\int_0^H T|_{r=R}\,\mathrm{d}z \tag{16}$$

$$\bar{q}''_{\mathrm{T}} = \frac{1}{\pi R^2}k\int_0^R \left.\frac{\partial T}{\partial z}\right|_{z=H} 2\pi r\,\mathrm{d}r, \quad \overline{T}_{\mathrm{T}} = \frac{1}{\pi R^2}\int_0^R T|_{z=H} 2\pi r\,\mathrm{d}r \tag{17}$$

$$\bar{q}''_{\mathrm{B}} = \frac{1}{\pi R^2}k\int_0^R \left.\frac{\partial T}{\partial z}\right|_{z=0} 2\pi r\,\mathrm{d}r, \quad \overline{T}_{\mathrm{B}} = \frac{1}{\pi R^2}\int_0^R T|_{z=0} 2\pi r\,\mathrm{d}r \tag{18}$$

The average heat transfer coefficient ($\bar{h}$) is expressed dimensionless form by the average Nusselt number ($\overline{Nu}$) obtained from Eq. (19) The characteristic length (L, Eq. (9)) takes into account the volume (V) and the total area (A_{Tot}) of the internal face of the tank.

$$\overline{Nu} = \frac{\bar{h}L}{k}, \quad L = \frac{V}{A_{\mathrm{Tot}}} \tag{19}$$

Fig. 6(a) shows the variation of the average Nusselt number ($\overline{Nu}$) as a function of the variation in average temperature, with curves referring to aspect ratios of 1, 1.5, 2, and 2.5. These cases have a global heat transfer coefficient (U^*), defined in Eq. (7), of 1.0 W/m^2 K, and a volume of 0.1 m^3.

Fig. 6(a) also shows that all results presented the same trend, despite deviate a determined value. This deviate refers to aspect ratio, and it was attenuated when the results of the average Nusselt number were multiplied by the aspect ratio to the power −0.3, as shown in Fig. 6(b).

It can be seen that the cases presented in Fig. 6(a) are different from those in Fig. 6(b). Both figures were selected as typical results, as all cases were grouped according to these two figures and present the same trend.

For each analyzed volume (0.1 and 0.2 m^3) and global heat transfer coefficient ($U^* = 1.0$, 1.3, 1.8, 2.9 and 8.0 W/m^2 K), the average of the values of

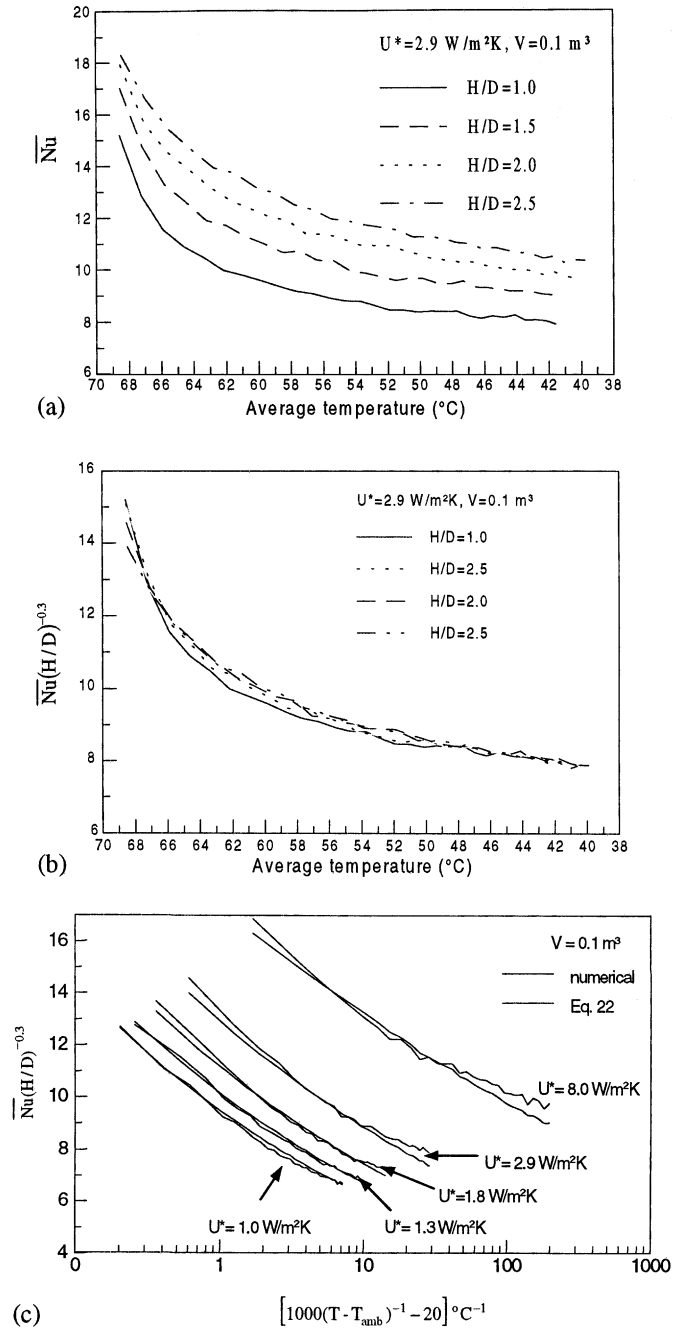

Fig. 6. Average Nusselt number: (a) $\overline{Nu}$ vs. average temperature, (b) $\overline{Nu}(H/D)^{-0.3}$ vs. average temperature; (c) $\overline{Nu}(H/D)^{-0.3}$ vs. $[1000(\overline{T}-T_{amb})^{-1}-20]\ ^{\circ}C^{-1}$.

$\overline{Nu}(H/D)^{-0.3}$ with results to the ratio aspects of 1, 1.5, 2 and 2.5 was taken, resulting in 10 average curves of $\overline{Nu}(H/D)^{-0.3}$. These curves were adjusted by the equation:

$$\overline{Nu}(H/D)^{-0.3} = AX^{B} \tag{20}$$

where A and B vary with the global heat transfer coefficient. The X variable is a function of the difference between the average temperature of the tank and the ambient temperature, and has the following form:

$$X = [1000(\overline{T}-T_{amb})^{-1}-20]^{\circ}C^{-1} \tag{21}$$

Aiming at generalizing the information, A and B were also adjusted. Coefficient A varies exponentially with U^* and B varies linearly with U^*.

Eq. (20), with already incorporates the coefficients corresponding to both analyzed volumes, is shown separately in Eqs. (22) and (23) for volumes of 0.1 and 0.2 m^3, respectively

$$\overline{Nu}(H/D)^{-0.3}_{V=0.1} = (9.40739U^{*0.288329})(1000(\overline{T} - T_{amb})^{-1} - 20)^{(0.00988842U^* - 0.189428)} \quad (22)$$

$$\overline{Nu}(H/D)^{-0.3}_{V=0.2} = (10.6039U^{*0.310719})(1000(\overline{T} - T_{amb})^{-1} - 20)^{(0.013052U^* - 0.224677)} \quad (23)$$

Calculating the coefficient of correlation among the 40 analyzed cases and those obtained by Eqs. (22) and (23), there was a variation between 0.979 and 0.998, showing an excellent consistency among the solutions, as shown in Fig. 6(c). The case that presented a coefficient of correlation of 0.979 corresponded to the volume of 0.2 m^3, with a global heat transfer coefficient (U^*) of 8.0 W/m^2 K. This small difference can be seen in Fig. 6(c).

The presented equations are valid for aspect ratios between 1 and 2.5. Although this is a wide range, there may be cases in engineering which use aspect ratios outside these limits. The authors believe that the presented equations may be also used in a wider aspect ratio, as the tested ratios were adjusted to a single curve when grouped under the power −0.3, as seen in Fig. 6(b). Obviously, there is a limit to the validity of this formulation when aspect ratios are so extreme that the diffusion vs. advection dynamics that are verified here cannot be applied.

6. Conclusions

The numerical and experimental results showed that, as time passes, there is a thermal stratification, separating the tank into two different regions: a stratified region (at the bottom) and another that it is uniform (at the top). The interface between these two regions advances towards the top. It was numerically verified that the tank under natural convection regime, in terms of convective flux direction, has two different regions. The region of descending flux direction has a ring shape along the walls, where heat is removed, replaced by the hydrodynamic boundary layer. The other is the central region, with very slow ascending flux, occupying almost 95% of the tank volume. At the periphery, thermal gradients are maximum, encompassing the thermal boundary layer. In the center, the thermal radial gradients are no existing.

The hydrodynamic boundary layer, created on the sidewall of the tank, can also be analyzed. During the first hour of cooling, the boundary layer is observed throughout the whole extension of this wall, but the most intense heat flux is located at the top portion of the tank. As time passes, diffusive and advective thermal processes became uncoupled, so the presence of the hydrodynamic boundary layer is observed only at the upper part of the tank.

The boundary condition of the third-kind is employed on the external face of the tank. The domain of calculation is extended up to the thermal insulation, taking also into account details of the metallic structure of the tank.

Aiming at validating the numerical simulation, experimental tests with different levels of initial temperature were carried out, with intervals of ≈10 °C between each test. All time levels were submitted to numerical simulation. Comparisons between the numerical simulations of a tank consisting of a metallic flange at the bottom and of another with glass-wool flange show the importance of thermal losses through the bottom of the tank. The tank with metallic flange at the bottom, besides cooling faster, presents a highly stratified temperature profile in this region, already during the first hours of cooling, whereas the temperature profile is only slightly stratified in the other case.

The tests with initial high temperatures have in common long cooling times (45 and 60 h), and excellent consistency between the numerical and experimental results. Both characteristics warrant the validation of the adopted numerical model. Therefore, taking also into account the independence of the adopted grids, it is concluded that the adopted model can be used to simulate similar situations with reliable results.

As previously seen, it may be concluded that the adopted methodology was able to describe in detail the phenomena that occur inside thermal tanks subjected to natural and mixed convection regime due to cooling or heating, with excellent consistency with the experimental results of temperature. It can be considered that these numerical results could only be obtained by the use of a complete and coupled formulation, including building details of the tank.

As the bi-dimensional numerical model was experimentally validated, the cooling of forty tanks with different aspect ratios, volumes and insulation thicknesses was simulated. These tests were submitted to the analysis of grid independence by GCI with a coefficient of safety ($F_s = 3$), providing maximum results in the order of 3%. The simulations estimated of the heat transfer of theses tanks and its dependence to the tank aspect ratio, the thermal loss to the environment, and the difference between the average temperature of the tank and environmental temperature in order to obtain a single equation for each of the tested volumes.

For the computation of the global heat transfer coefficient U^*, the thermal resistance by convection on the external side of the wall, and the diffusion heat transfer

resistance inside the thermal insulation are taken into consideration. Considering that the dominant resistance in most of the studied cases is diffusive, the external wall convective heat transfer coefficient, being less significant, can vary according to the angle, for instance, without causing large variations in U^*. Therefore, it was concluded that the presented results are independent of the external convective pattern. On the other hand, variations in insulation thickness (side, top and bottom) can significantly affect U^*. Finally, it must be observed that, in practical applications, tanks usually have the same insulation thickness in the top, bottom and sides, which were covered in this analysis.

Acknowledgements

The authors are grateful to the Brazilian CAPES and CNPq for the financial support to this work.

References

[1] D.T. Reindl, W.A. Beckman, J.W. Mitchell, Transient natural convection in enclosures with application to solar thermal storage tanks, Solar Eng. 2 (1992) 1143–1148.
[2] M.A. Cotter, M.E. Charles, Transient cooling of petroleum by natural convection in cylindrical storage tanks—II. Effect of heat transfer coefficient, aspect ratio and temperature—Dependent viscosity, Int. J. Heat Mass Transfer 36 (1992) 2175–2182.
[3] W. Lin, S.W. Armfiel, Direct simulation of natural convection cooling in a vertical circular cylinder, Int. J. Heat Mass Transfer 42 (1999) 4117–4130.
[4] A. Ivancic, A. Oliva, C.D. Péres-Segarra, M. Costa, Heat transfer in vertical cylindrical enclosures for supercritical Rayleigh number and arbitrary side-wall conductivity, Int. J. Heat Mass Transfer 42 (1999) 332–343.
[5] E.M Kleinbach, W.A. Beckman, S.A. Klein, Performance study of one-dimensional models for stratified thermal storage tanks, Solar Energy 2 (1993) 155–166.
[6] R. Franke, Object-oriented modeling of solar heating systems, Solar Energy 60 (1997) 171–180.
[7] R.J. Gross, An experimental study of single medium thermocline termed energy storage, ASME Report 82-HT-53 (1983) 1–8.
[8] Y.H. Zurigat, P.R. Liche, A.J. Ghajar, Influence of inlet geometry on mixing in thermocline thermal energy storage, Int. J. Heat Mass Transfer 34 (1991) 115–125.
[9] S.S. Murthy, J.E.B. Nelson, L.S. Rao, Effect of wall conductivity on thermal stratification, Solar Energy 49 (1992) 273–277.
[10] J.E.B. Nelson, A.R. Balakrishnan, S.S. Murthy, Experiments on stratified chilled-water tanks, Int. J. Refrig. 22 (1999) 216–234.
[11] F.J. Oppel, A.J. Ghajar, P.M. Moretti, A numerical and experimental study of stratified thermal storage, ASHRAE Trans., Part A 92 (1986) 293–309.
[12] R.L. Cole, F.O. Bellinge, Thermally stratified tanks, ASHRAE Trans., Part A 94 (1988) 1005–1017.
[13] N.M. Al-Najem, A.M. Al-Marafie, K.Y. Ezuddin, Analytical and experimental investigation of thermal stratification in storage tanks, Int. J. Energy Res. 176 (1992) 77–88.
[14] R.J. Moffat, Describing the uncertainties in experimental results, Expt. Thermal Fluid Sci. 1 (1988) 3–17.
[15] R.S. Adihkari, A. Kumar, G.D. Sootha, Simulation studies on a multi-stage stacked tray solar still, Solar Energy 54 (1995) 317–325.
[16] S.V. Patankar, Numerical Heat Transfer and Fluid Flow, McGraw-Hill, 1980.
[17] H.K. Versteeg, W. Malalasekera, An Introduction to Computational Fluid Dynamics—The Finite Volume Method, Longman Scientific & Technical, 1995.
[18] J.H. Ferziger, M. Periç, Computational Methods for Fluid Dynamics, Springer, 1997.
[19] J.P. Van Doormaal, G.D. Raithby, Enhancements of the simple method for predicting incompressible fluid flow, Num. Heat Transfer 7 (1984) 147–163.
[20] S.V. Patankar, A calculation procedure for two-dimensional elliptic situations, Num. Heat Transfer 2 (1979) 417–440.
[21] P.J. Roache, Verification and Validation in Computational Science and Engineering, Hermosa Publishers, 1998.
[22] L. Davidson, Calculation of the turbulence buoyancy-driven flow in a rectangular cavity using an efficient solver and two different low Reynolds number κ–ε turbulence models, Num. Heat Transfer 18 (1990) 129–147.
[23] M.A. Bandini, H.A. Vielmo, Numerical analysis of velocity and temperature in storage tanks of solar systems, Renew. Energy 15 (1998) 2080–2083.
[24] M.A. Abdoly, D. Rapp, Theoretical and experimental studies of stratified thermocline storage of hot water, Energy Convers. Mgmt. 22 (1982) 275–285.
[25] S. Kimura, A. Bejan, Natural convection in a differentially heated corner region, Phys. Fluids 28 (1985) 2980–2989.
[26] R. De C. Oliveski. Análise Numérica Experimental dos Campos de Temperatura e Velocidade em Armazenadores Térmicos. Doctoral Thesis, Federal University of Rio Grande of Sul, PROMEC, Brazil, 2000.